IOP Publishing Plasma Physics and Controlled Fusion
Plasma Phys. Control. Fusion **62** (2020) 025030 (11pp) https://doi.org/10.1088/1361-6587/ab60ff

Role of Hall effect on the resistive kink mode in tokamaks

W Zhang, Z W Ma, H W Zhang and X Wang

Institute for Fusion Theory and Simulation, Department of Physics, Zhejiang University, Hangzhou 310027, People's Republic of China

E-mail: zwma@zju.edu.cn

Received 18 September 2019, revised 9 December 2019
Accepted for publication 11 December 2019
Published 9 January 2020

Abstract

The influence of the Hall effect on the nonlinear evolution of the $m/n = 1/1$ resistive-kink mode is numerically investigated by the three-dimensional toroidal Hall-MHD code CLT. It is found that the Hall effect can lead to the explosive growth of the resistive-kink mode at the nonlinear stage. The explosive nonlinear growth of the resistive-kink mode mainly results from the structural transition of the current sheet in the Hall-MHD simulations. At the nonlinear stage, the geometry of the current sheet turns into X-type from Y-type, resulting in the significant acceleration of the reconnection process. The fast reconnection induced by the Hall effect may explain the fast crash observed in large tokamaks. We also found that there exists a critical value of the ion inertial length that is resulted from the acceleration of magnetic reconnection due to the decoupling motions of ions and electrons and the suppression effect by the electron diamagnetic rotation in the Hall MHD. The critical value of d_i decreases with increasing thermal conductivity $\kappa_\perp$. When d_i exceeds a critical value, the peak growth rate decreases with increasing d_i.

Keywords: Hall, sawtooth, crash, electron diamagnetic drift, GPU

(Some figures may appear in colour only in the online journal)

1. Introduction

Sawtooth in magnetically confined fusion devices (such as tokamaks) is periodic oscillations of the core temperature with a rapid drop (about 10–100 μs) after a slow rise (about a few milliseconds) [1–3]. Sawtooth is one of the most common phenomena in tokamaks when the safety factor on the magnetic axis is below 1.0. Sawtooth plays an important role in Tokamak performance because it can trigger neo-classical tearing mode instabilities [4, 5] on other rational surfaces, which are very deleterious for plasma confinement. It can also influence the confinement of α particles [6]. Therefore, for magnetically confined fusion reactors, it is crucial to understand the physical mechanism behind sawtooth oscillations.

Sawtooth was firstly observed in 1974 in the symmetric Tokamak [1]. Kadomtsev [7] then proposed a complete reconnection model to explain the temperature crash in the core region with the crash time $\tau_c \sim (\tau_A \tau_R)^{1/2}$, where τ_A and τ_R are the Alfvén and resistive diffusion times, respectively. However, as plasmas become hotter in large tokamaks (such as JET [8] and TFTR [9]), the resistivity of plasmas in these experiments becomes lower. Therefore, the crash time predicted in the Kadomtsev's model is about two orders of magnitude larger than the observed crash times. In order to resolve this big difference, many works on sawtooth [4, 10–40] have been carried out.

Aydemir [15] firstly found that the $m/n = 1/1$ resistive kink mode exhibits a nonlinearly enhanced growth rate that far exceeds its linear growth rate due to collisionless modification in the four-field model given by Hazeltine *et al* [41]. Shortly after that, Wang and Bhattacharjee [16] presented an analytical theory for the nonlinear dynamical evolution of the $m/n = 1/1$ resistive kink mode, governed by the Hall term. It successfully explains the nonlinearly enhanced growth rates -the acceleration of reconnection results from the geometry transition in the reconnection diffusion region. In the framework of resistive-MHD, which does not include Hall terms, the current sheet becomes thinner and elongated at the nonlinear stage. The current sheet then looks like two 'Y' characters. That is why it is called Y-type reconnection. The

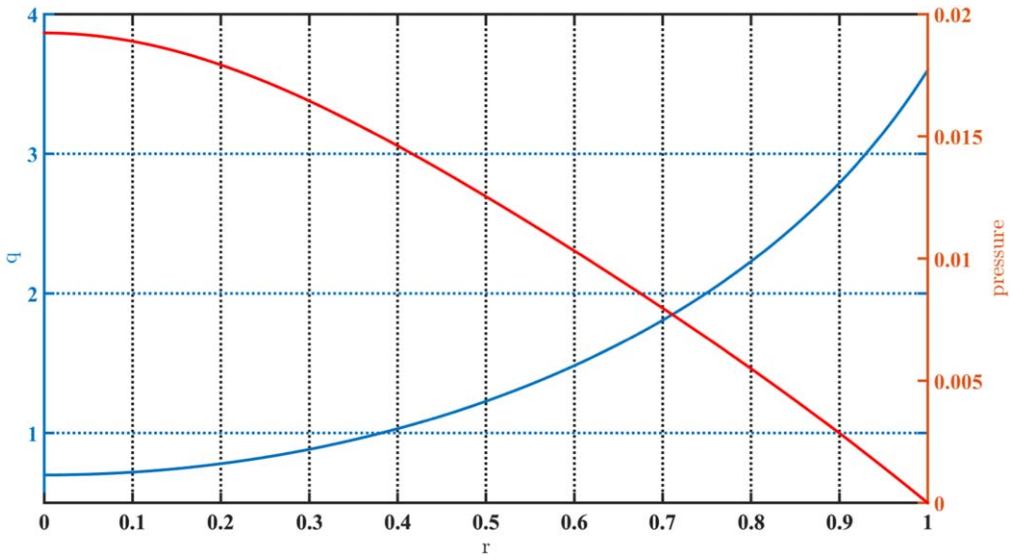

Figure 1. The initial q and pressure profiles. $r = \sqrt{\psi_{norm}}$, where ψ_{norm} is the normalized magnetic flux.

Y-type current sheet implies that the time scale of magnetic reconnection will be slow [42]. However, in the framework of Hall-MHD, the current sheet shrinks and its length becomes in the same order of the current thickness, which looks like an 'X' character. Such geometry transition in the nonlinear stage results in the fast reconnection process [43–46]. However, these studies are either based on the reduced MHD model in the cylindrical geometry or carried out with compressible Hall MHD model in the slab geometry, and a toroidal investigation is then needed to ensure that the fast crash observed in tokamaks is indeed related to Hall effects. However, three-dimensional (3D) Hall MHD simulations in the toroidal geometry are not easy to be conducted. The difficulty of a 3D Hall MHD simulation is that the Hall term can introduce a dispersive dispersion relation $\omega \sim k^2$ that causes severe problems on the numerical stability [47, 48]. Recently, Beidler *et al* firstly presented 3D toroidal Hall-MHD simulations on the fast reconnection during the sawtooth crash through an implicit code M3D-C1 [20]. In the present paper, we will carry out our 3D toroidal Hall-MHD simulations by an explicit code.

2. The Hall-MHD model in CLT

The CLT code is a three-dimensional toroidal Hall-MHD code. The 4th order finite difference method in the R, ϕ, and Z directions, and the 4th order Runge–Kutta scheme in the time integration are applied [49]. In CLT, the cut-cell method is used to handle the boundary problems [50]. The full set of the Hall-MHD equations used in the CLT code is given as follows:

$$\frac{\partial \rho}{\partial t} = -\nabla \cdot (\rho \mathbf{v}) + \nabla \cdot [D\nabla(\rho - \rho_0)], \tag{1}$$

$$\frac{\partial p}{\partial t} = -\mathbf{v} \cdot \nabla p - \Gamma p \nabla \cdot \mathbf{v} + \nabla \cdot [\kappa \nabla (p - p_0)], \tag{2}$$

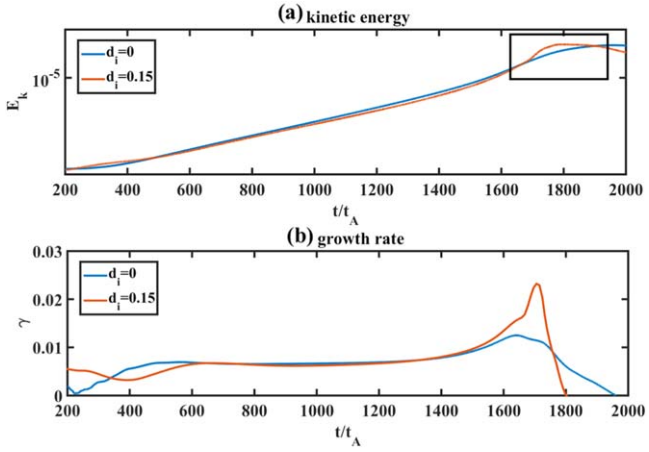

Figure 2. The evolutions of (a) the kinetic energy and (b) the growth rate for the $m/n = 1/1$ resistive-kink mode with and without the Hall effect. The kinetic energy is normalized with $\rho_0 V_A^2$.

$$\frac{\partial \mathbf{v}}{\partial t} = -\mathbf{v} \cdot \nabla \mathbf{v} + (\mathbf{J} \times \mathbf{B} - \nabla p)/\rho + \nabla \cdot [\upsilon \nabla (\mathbf{v} - \mathbf{v}_0)], \tag{3}$$

$$\frac{\partial \mathbf{B}}{\partial t} = -\nabla \times \mathbf{E}, \tag{4}$$

$$\mathbf{E} = -\mathbf{v} \times \mathbf{B} + \eta(\mathbf{J} - \mathbf{J}_0) + \frac{d_i}{\rho}(\mathbf{J} \times \mathbf{B} - \nabla p), \tag{5}$$

$$\mathbf{J} = \frac{1}{\mu_0} \nabla \times \mathbf{B}, \tag{6}$$

where ρ, p, p_e, $\mathbf{v}$, $\mathbf{B}$, $\mathbf{E}$, and $\mathbf{J}$ are the mass density, the total plasma pressure, the electron pressure, the plasma velocity, the magnetic field, the electric field, and the current density, respectively. The plasma pressure is contributed only from electrons due to the assumption of cold ions, i.e. $p = p_e$. The subscript '0' means the initial value. $\Gamma(=5/3)$ is the ratio of specific heat of plasma. The normalization of the variables used in the present paper are: $\mathbf{B}/B_{00} \rightarrow \mathbf{B}$, $\mathbf{x}/a \rightarrow \mathbf{x}$, $\rho/\rho_{00} \rightarrow \rho$,

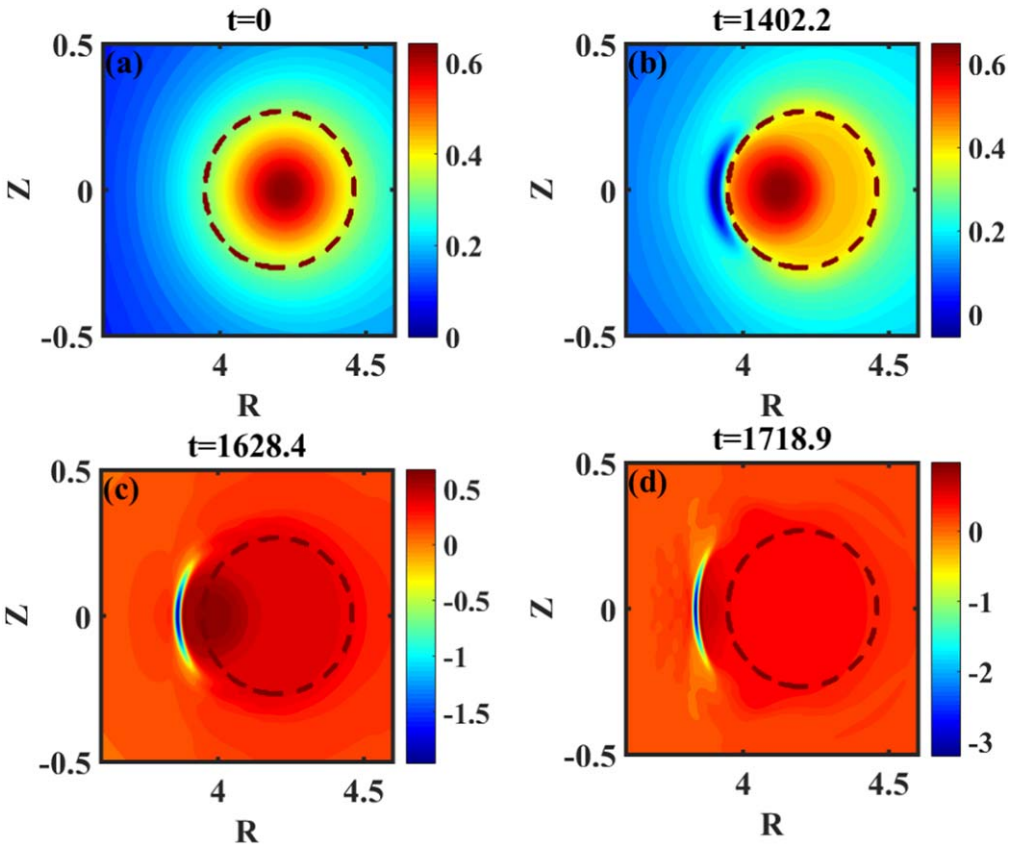

Figure 3. The snapshots of the contour plots of the toroidal current density in the resistive-MHD simulation in the poloidal plane with $\phi = 0$ at (a) $t = 0t_A$, (b) $t = 1402.2t_A$, (c) $t = 1628.4t_A$, and (d) $t = 1718.9t_A$. The dark red dashed line is the initial $q = 1$ surface.

$\mathbf{v}/v_A \rightarrow \mathbf{v}$, $t/t_A \rightarrow t$, $p/(B_{00}^2/\mu_0) \rightarrow p$, $\mathbf{J}/(B_{00}/\mu_0 a) \rightarrow \mathbf{J}$, and $\mathbf{E}/(v_A B_{00}) \rightarrow \mathbf{E}$, where a is the minor radius, $v_A = B_{00}/\sqrt{\mu_0 \rho_{00}}$ is the Alfvén speed, and $t_A = a/v_A$ is the Alfvén time. B_{00} and ρ_{00} are the initial magnetic field and mass density at the magnetic axis, respectively. $d_i = c/\omega_{pi}$ is the ion inertial length, where ω_{pi} is the ion plasma frequency. η, D, $\kappa_\perp$, $\kappa_\parallel$, and υ are the resistivity, the plasma diffusion coefficient, the perpendicular and parallel thermal conductivity, and the viscosity, respectively, and normalized as follows: $\eta/(\mu_0 a^2/t_A) \rightarrow \eta$, $D/(a^2/t_A) \rightarrow D$, $\kappa_\perp/(a^2/t_A) \rightarrow \kappa_\perp$, $\kappa_\parallel/(a^2/t_A) \rightarrow \kappa_\parallel$, and $\upsilon/(a^2/t_A) \rightarrow \upsilon$.

3. Simulation results

3.1. Fast reconnection induced by Hall effect

A toroidal Tokamak geometry with a circular cross-section is chosen in our simulations (the major radius $R_0 = 4$ and the minor radius $a = 1$). The initial safety factor and pressure profiles are shown in figure 1. Since the safety factor at the magnetic axis is $q_0 = 0.7$, the most unstable mode in the system is the $m/n = 1/1$ resistive kink mode. The equilibrium is obtained from the NOVA code [51]. The benchmarking could be seen from our previous studies [52]. The grids used in the present paper are $400 \times 64 \times 400$ (R, ϕ, Z). Since there are 64 grids in the ϕ direction, the maximum toroidal mode number is 32. The convergence studies have been ensured by using different grids, i.e. $256 \times 64 \times 256$, $400 \times 64 \times 400$, and $400 \times 128 \times 400$ (R, ϕ, Z), respectively. In the present paper, the resistivity, the viscosity, the plasma diffusivity, the parallel and perpendicular thermal conductivity, are chosen to be $\eta = 3 \times 10^{-6}$, $\upsilon = 3 \times 10^{-5}$, $D = 1.0 \times 10^{-4}$, $\kappa_\parallel = 5 \times 10^{-2}$, and $\kappa_\perp = 3.0 \times 10^{-5}$ to $\kappa_\perp = 3.0 \times 10^{-7}$, respectively. The resistivity in the present paper is constant and remains unchanged during the simulation. The purpose for the constant resistivity is to clearly show the significant influence of the Hall effect on the resistive kink mode.

In this subsection, we conduct two typical cases with $d_i = 0$ (resistive-MHD) and $d_i = 0.15$ (Hall-MHD) to illustrate influences of the Hall effect on the nonlinear evolution of the $m/n = 1/1$ resistive-kink mode. The evolutions of the kinetic energy and the growth rate for the $m/n = 1/1$ resistive-kink mode with and without the Hall effect are shown in figure 2. In the present paper, the growth rate is defined as $\gamma = \partial(\ln E_k)/\partial t$, and is normalized with t_A^{-1}, where t_A is the Alfven time. The linear growth rates for the two cases are both about 0.006. In the nonlinear stage, the growth rates of the kinetic energy in both cases exhibit enhancement. In the resistive case, the enhancement of the nonlinear growth rate is associated with that magnetic reconnection is accelerated by the external inward flow [53] induced by internal kink instability. In the Hall case, the burst in the nonlinear phase results from both external inward flow and the Hall effects

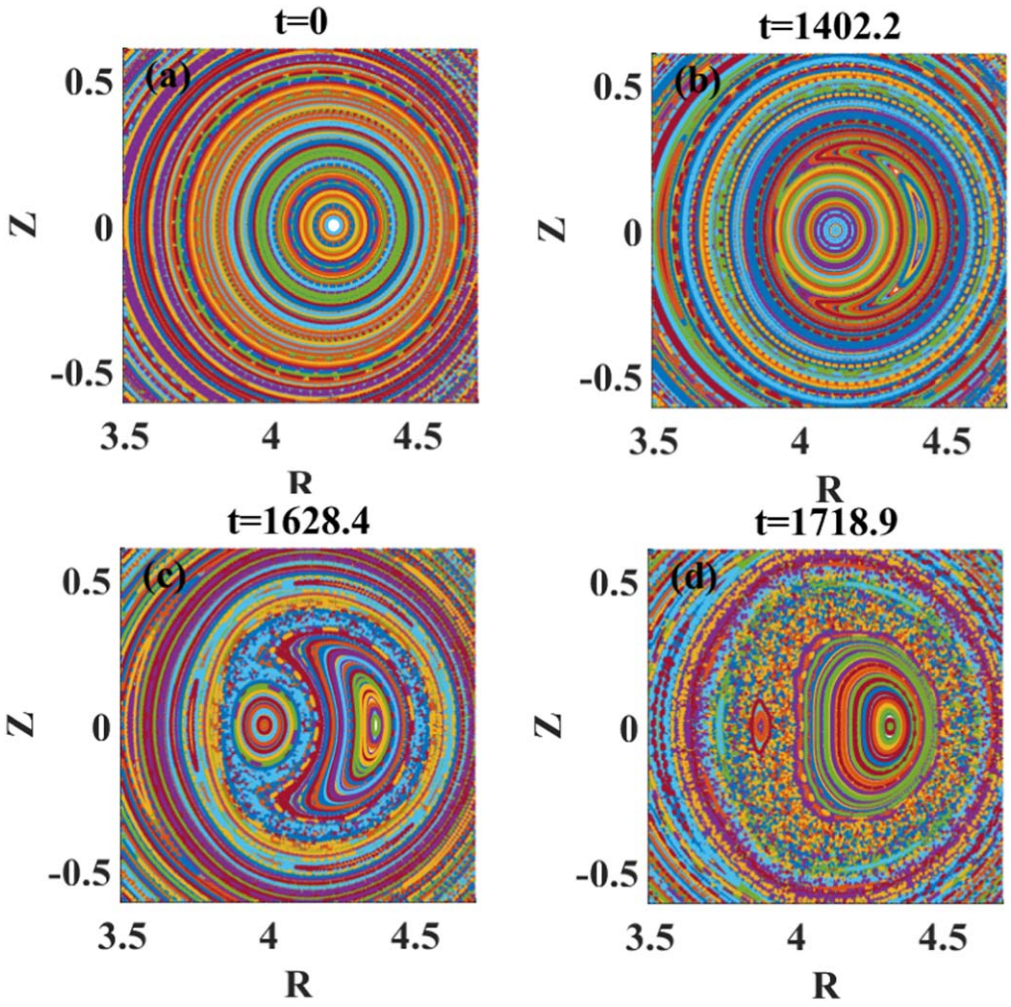

Figure 4. The Poincaré plots of the magnetic field in the Hall-MHD simulation in the poloidal plane with $\phi = 0$ at (a) $t = 0t_A$, (b) $t = 1402.2t_A$, (c) $t = 1628.4t_A$, and (d) $t = 1718.9t_A$.

[46]. Hall terms can lead to the separated motion of ions and electrons in the vicinity of the diffusion region with the spatial scale d_i. The influence of the Hall effect can be dominant when the current sheet is sufficiently thin. As a result, the elongated thin current sheet shrinks, and the reconnection rate exhibits a significant enhancement. The maximum growth rate for the case with $d_i = 0.15$ is about 0.026, which is four times larger than its linear growth rate. These results agree well with previous cylindrical simulations [15] and theoretical analysis [16].

Figure 3 shows the snapshots of the toroidal current density in the resistive-MHD simulation. It indicates that the reconnection in the diffusion region keeps Sweet-Parker [42] (or called Y-type) reconnection throughout the evolution of the resistive-kink mode. The current sheet is thin and strong at the nonlinear stage, as shown in figure 3(d). It could also be seen from the Poincare plots of the magnetic field (figure 4). With the Hall effect, the current sheet structure at the linear and early nonlinear stage is similar to that in resistive-MHD simulation, as shown in figures 5(a) and (b). However, when the thickness of the current sheet reduces to a critical value, the Hall terms start to play a dominant role during the reconnection. Then the elongated thin current sheet shrinks, and the current sheet geometry in the diffusion region turns into the X-type from the Y-type (figures 5(c) and (d)). Since the X-type reconnection could be much faster than the Y-type reconnection, the kinetic energy experiences explosive growth, and the maximum reconnection rate in the nonlinear stage becomes much larger than that in the linear stage.

The evolution of the growth rate for the resistive-MHD and Hall-MHD simulations are shown in figures 6(a) and (b). At the linear stage, the harmonics ($m/n \neq 1/1$) are resulted from the nonlinear interaction of the $m/n = 1/1$ mode for both resistive-MHD simulations and Hall-MHD simulations, since their growth rates are approximately equal to multiple times of the growth rate of $m/n = 1/1$ mode ($\gamma_{m/n} = n\gamma_{m/n=1/1}$). However, the behavior of the harmonics could be extremely different at the nonlinear stage. For the resistive-MHD simulations, the nonlinear growth rates of the harmonics of the $m/n = 1/1$ mode decrease. However, in the Hall-MHD simulations, the growth rates of the harmonics of the $m/n = 1/1$ mode significantly increase at the nonlinear stage, which suggests that the explosive growth at the nonlinear stage is mainly due to the fast development of the harmonics of the $m/n = 1$ mode.

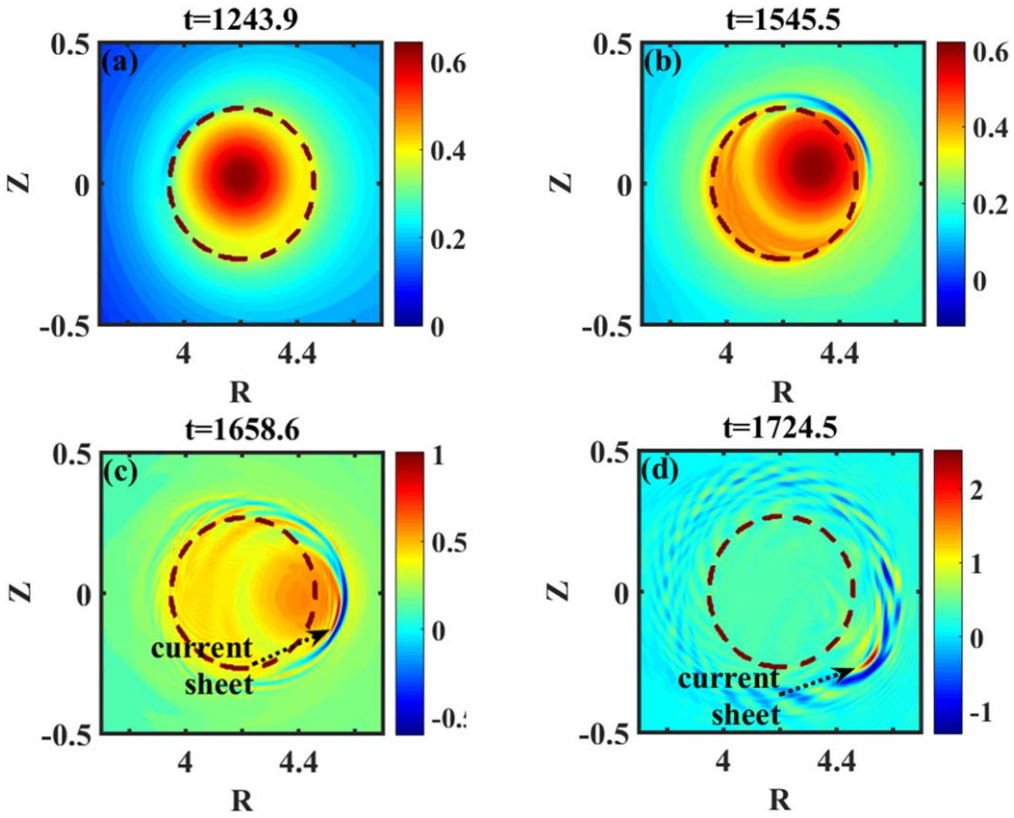

Figure 5. The snapshots of the contour plots of the toroidal current density in the Hall-MHD simulation in the poloidal plane with $\phi = 0$ at (a) $t = 1243.9t_A$, (b) $t = 1545.5t_A$, (c) $t = 1658.6t_A$, and (d) $t = 1724.5t_A$. The dark red dashed line is the initial $q = 1$ surface.

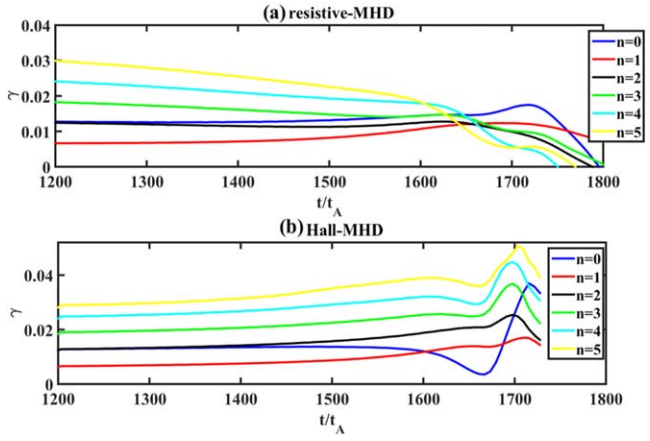

Figure 6. The evolution of the growth rate for modes with different toroidal numbers (a) the resistive-MHD and (b) the Hall-MHD simulations.

The mode structures of the resistive-kink mode at the time with the maximum growth rate for (a) resistive-MHD and (b) Hall-MHD are shown in figure 7. The higher harmonics of the $m/n = 1/1$ mode are also well developed at the nonlinear stage. In the framework of resistive-MHD, the amplitudes of the $m/n = 2/2$ and $3/3$ modes are lower than that of the $m/n = 1/1$ mode. However, in the Hall-MHD simulations, the amplitudes of the $m/n = 2/2$ and $3/3$ modes become larger than that of the $m/n = 1/1$ mode. The energy spectrums are shown in figure 8(a) resistive-MHD and (b) Hall-MHD, which also indicates that both the $m/n = 1/1$ mode and its higher harmonics become dominant, and even much higher harmonics of the $m/n = 1/1$ mode appear in Hall-MHD simulations.

It should be noted that the current sheet rotates in the clockwise direction with $d_i = 0.15$ (figure 5), which means that the resistive-kink mode has a real frequency in Hall-MHD simulations. The mode rotation could also be seen from the Poincaré plots of the magnetic field (figure 9). However, the real frequency is zero in resistive-MHD simulations (figures 3 and 4). The real frequency of the resistive-kink mode results from the electron diamagnetic drift introduced by Hall terms. Since the electron diamagnetic drift frequency $\omega_{*e} = -\frac{m}{n_0 e r B_T}\frac{dp_e}{dr}$ is proportional to the poloidal mode number m, the harmonics of the $m/n = 1/1$ mode have different rotation frequency. That is the reason why there exists some 'ripple' on the contour plot of toroidal current at the nonlinear stage (figures 5(b) and (c)).

The contour images of the pressure and the safety factor q at the nonlinear stage in the Hall-MHD simulations are shown in figure 10. At $t = 1658.6t_A$, the safety factor at the magnetic axis is about 0.7, which is the same with the initial value (figure 10(c)). After the reconnection, the minimum q in the whole region becomes 1.0 (figure 10(d)), which indicates that it is a complete reconnection. At $t = 1724.5t_A$, the original core is squeezed to the X-point and almost disappears. As a result, a peak of pressure profiles forms near X-point (figure 10(b)), and

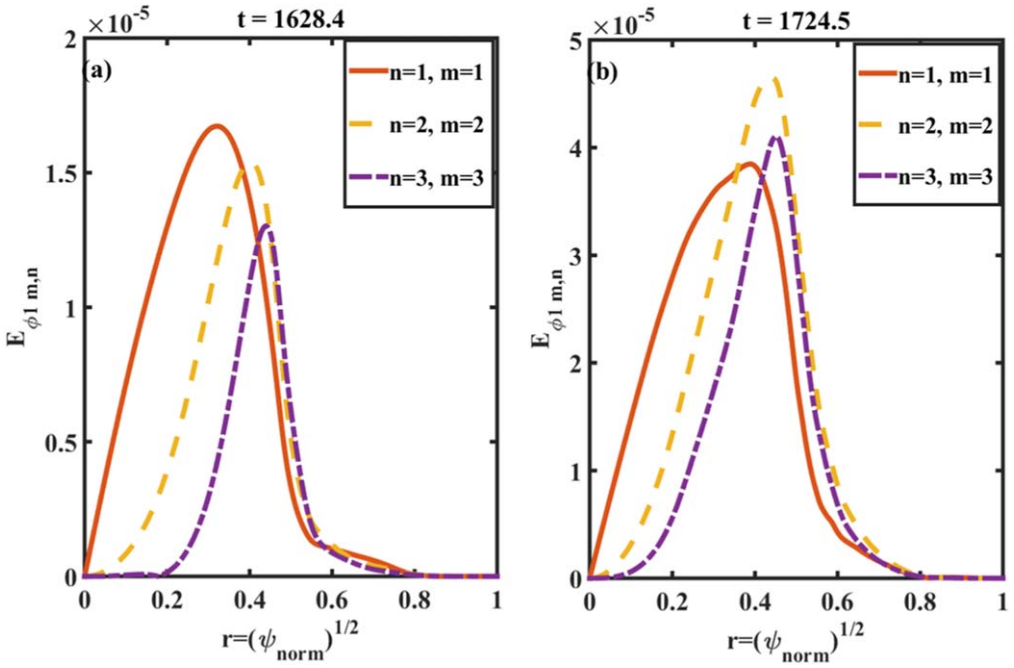

Figure 7. The mode structures of the resistive-kink mode at the time with the maximum growth rate for (a) resistive-MHD and (b) Hall-MHD.

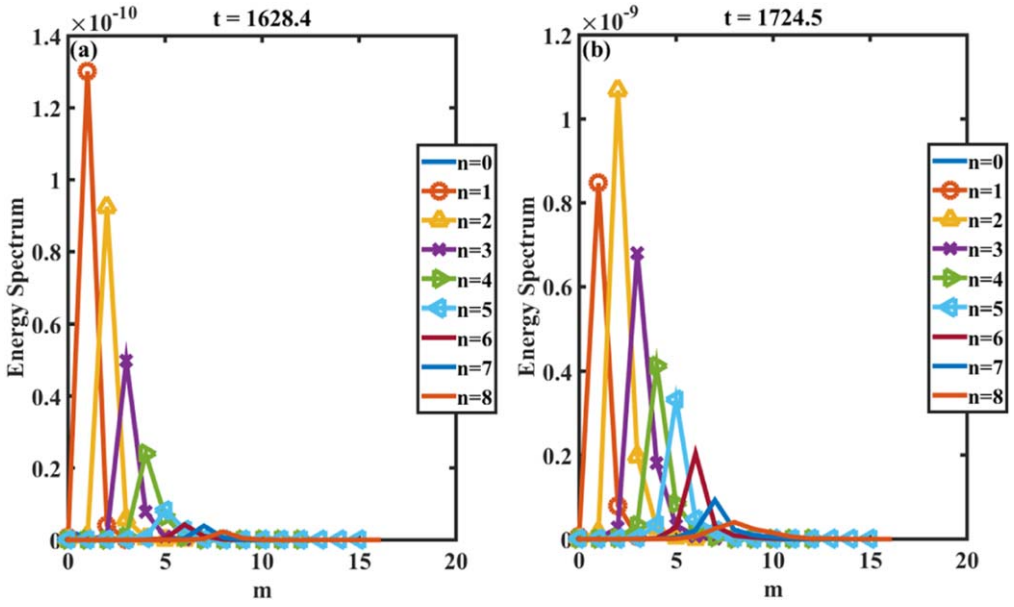

Figure 8. The energy spectrum (kinetic energy) of the resistive-kink mode at the time with the maximum growth rate for (a) resistive-MHD and (b) Hall-MHD.

the plasma pressure becomes almost flattened in other regions. However, due to the stochasticity of the magnetic field in the broad region, the original core could not be clearly seen from the Poincare plots (figure 9(d)) or the safety factor image (figure 10(d)). The stochasticity of the magnetic field mainly results from the development of different helical modes.

3.2. The nonlinear evolution of the resistive-kink mode with different d_i

The inclusion of Hall terms in the generalized Ohm's law leads to two effects: the electron diamagnetic drift [54], which could reduce the growth rate of the resistive-kink mode, and the structural transition of the thin current sheet [16], which could significantly enhance the nonlinear reconnection rate. For typical parameters in the present tokamaks, the particle density is about $n = 2{-}4 \times 10^{19}\ \mathrm{m}^{-3}$, the ion plasma frequency is about $\omega_{pi} = 0.6 - 0.8 \times 10^{10}\ \mathrm{s}^{-1}$, the minor radius is $a \sim 0.5$ and $c = 3 \times 10^{8}\ \mathrm{m\,s}^{-1}$, then we have $d_i = c/\omega_{pi} = 4{-}5$ cm and $d_i/a \sim 0.1$. As a result, the range of the ion inertial length in the present subsection is scanned from $d_i = 0$ to $d_i = 0.2$. The linear growth rates of the resistive-kink mode with different $\kappa_\perp$ and d_i are shown in figure 11, which is similar to our previous studies [55].

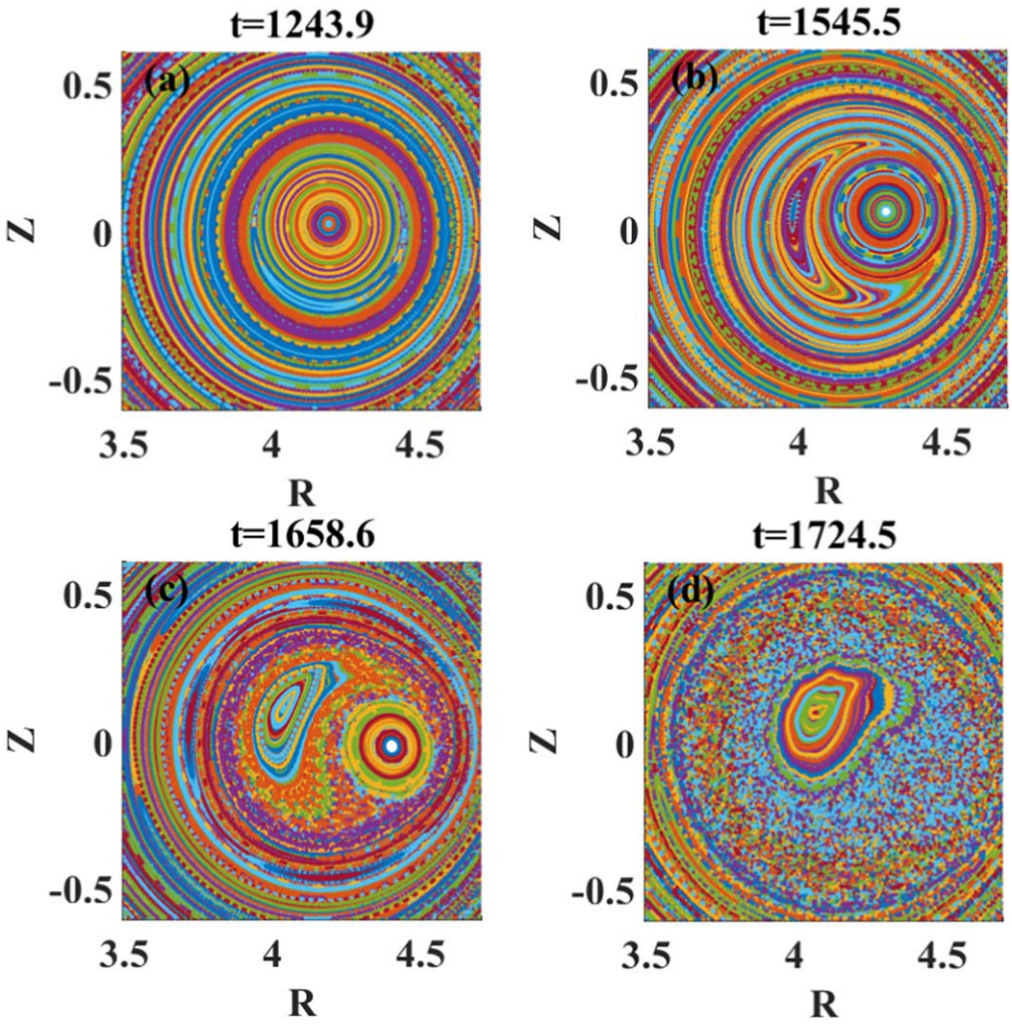

Figure 9. The Poincaré plots of the magnetic field in the Hall-MHD simulation in the poloidal plane with $\phi = 0$ at (a) $t = 1243.9t_A$, (b) $t = 1545.5t_A$, (c) $t = 1658.6t_A$, and (d) $t = 1724.5t_A$.

The evolutions of the growth rates with $\kappa_\perp = 3 \times 10^{-6}$ and different d_i are shown in figure 12. It is found that, for the cases with $d_i < 0.12$, the maximum nonlinear growth rate increases with increasing d_i. However, for the cases with $d_i > 0.12$, the maximum nonlinear growth rate decreases with increasing d_i.

It should be noted that the electron diamagnetic drift velocity is proportional to d_i, and it can significantly suppress the resistive-kink mode when the perpendicular thermal conductivity is large while the electron magnetic drift only has little influence on the growth rate of the resistive-kink mode when $\kappa_\perp$ is small. It implies that the critical value of d_i is due to the competition between the suppression by the electron diamagnetic rotation and the acceleration of magnetic reconnection by decoupling motions of ions and electrons in the Hall MHD.

As indicated in figure 11, the electron magnetic drift only has little influence on the growth rate of the resistive-kink mode with a small thermal conductivity. Therefore, we further conduct the cases with $\kappa_\perp = 3 \times 10^{-7}$ and different d_i to show the acceleration of magnetic reconnection by the Hall effect. From figure 13, the maximum growth rate in the case with $d_i = 0.2$ is about 0.029, which is only slightly smaller than that with $d_i = 0.15$ (the maximum growth rate is about 0.031). When $\kappa_\perp = 3 \times 10^{-5}$, the maximum growth rate with $d_i = 0.15$ is even smaller than that in the resistive-MHD simulation (figure 14). With $d_i = 0.2$, the linear growth rate of the resistive-kink mode further decreases to 0.001, which means that the mode is almost fully suppressed by the electron diamagnetic drift. The simulation results for the cases with $\kappa_\perp = 3 \times 10^{-7}$ and $\kappa_\perp = 3 \times 10^{-5}$ in figures 13 and 14 suggest that as d_i increases, the decrease of the maximum nonlinear growth rate is mainly due to the increase of the electron diamagnetic rotation.

A series of numerical simulations with the application of GPU acceleration [49] is carried out to study the nonlinear dynamics of the resistive kink mode under different ion inertial length and the perpendicular thermal conductivities. It is found that the Hall effect can lead to the explosive growth of the resistive-kink mode at the nonlinear stage, which agrees well with previous theoretical predictions [16] and simulation results [20, 38]. The acceleration of reconnection results from

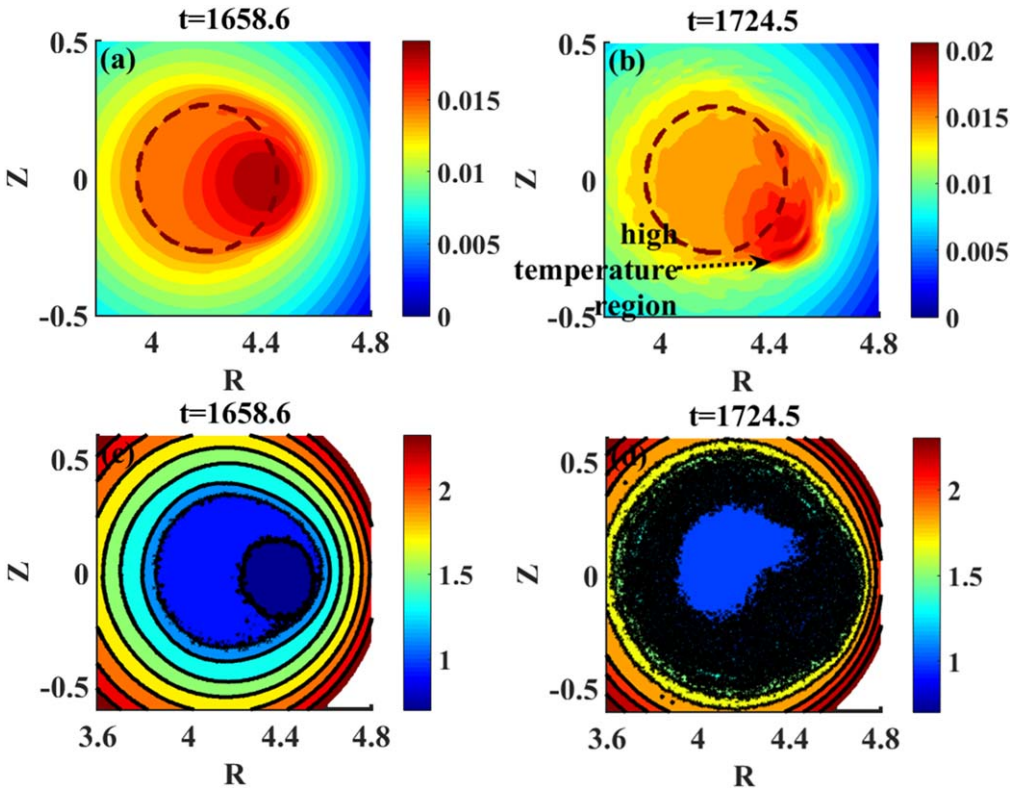

Figure 10. The contour plot of the total plasma pressure at (a) $t = 1658.6t_A$, and (b) $t = 1724.5t_A$ in the poloidal plane with $\phi = 0$. The dark red dashed line is the initial $q = 1$ surface. The contour plot of safety factor profiles in the poloidal plane with $\phi = 0$ at (c) $t = 1658.6t_A$, and (d) $t = 1724.5t_A$.

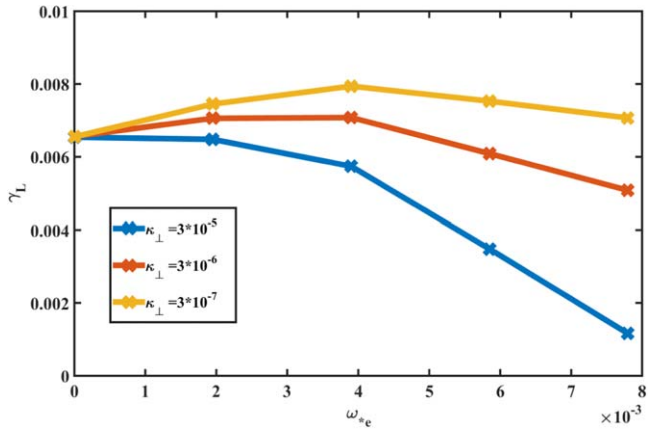

Figure 11. The linear growth rates of the resistive-kink mode with different $\kappa_\perp$ and d_i.

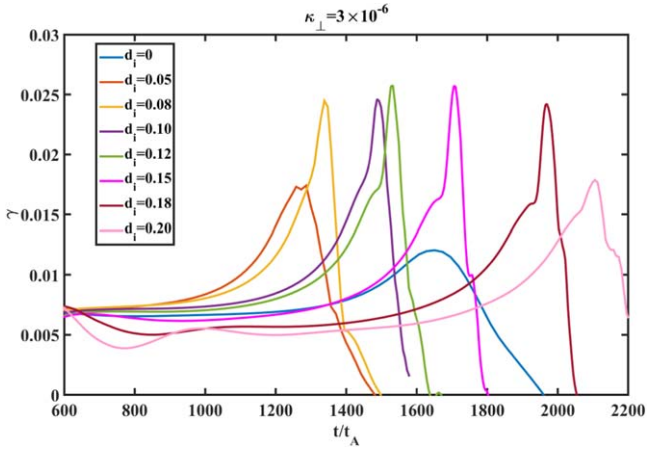

Figure 12. The evolutions of the growth rates with $\kappa_\perp = 3 \times 10^{-6}$ and different d_i. It should be noted that, for the cases with $d_i < 0.12$, the maximum nonlinear growth rate increases with increasing d_i. However, for the cases with $d_i > 0.12$, the maximum nonlinear growth rate decreases with increasing d_i.

the geometry transition in the reconnection diffusion region. In the framework of resistive-MHD, the current sheet becomes thinner and elongated. The geometry of the current sheet remains Y-type during the nonlinear evolution of the resistive-kink mode. However, in the framework of Hall-MHD, the length of the current sheet shrinks, and the geometry of the diffusion region changes from Y-type to X-type at the nonlinear stage, resulting in a fast reconnection process. It is also found that the increase of the ion inertial length (d_i) does not always lead to an increase of the nonlinear growth rate. When d_i is smaller than the critical value, the maximum growth rate increases with increasing d_i; however, when d_i is larger than the critical value, the maximum growth rate decreases with increasing d_i. It is due to competition between the suppression by the electron diamagnetic drift and the acceleration by the Hall effect. Besides, the perpendicular thermal conductivity $\kappa_\perp$ is also found to have a significant

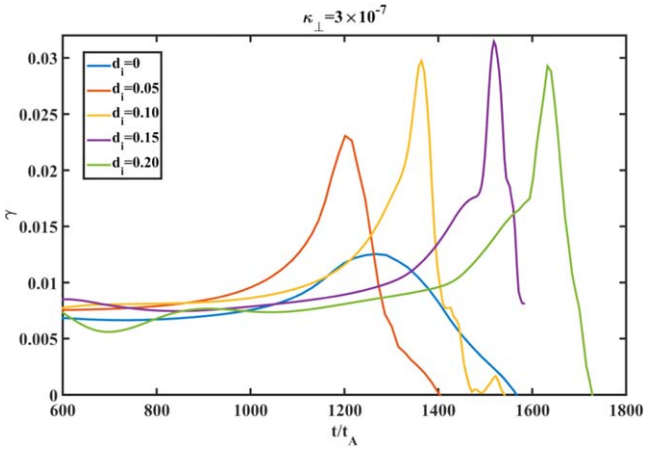

Figure 13. The evolutions of the growth rates with $\kappa_\perp = 3 \times 10^{-7}$ and different d_i. For the cases with $d_i < 0.15$, the maximum nonlinear growth rate increases with increasing d_i. After that, the maximum nonlinear growth slightly decreases.

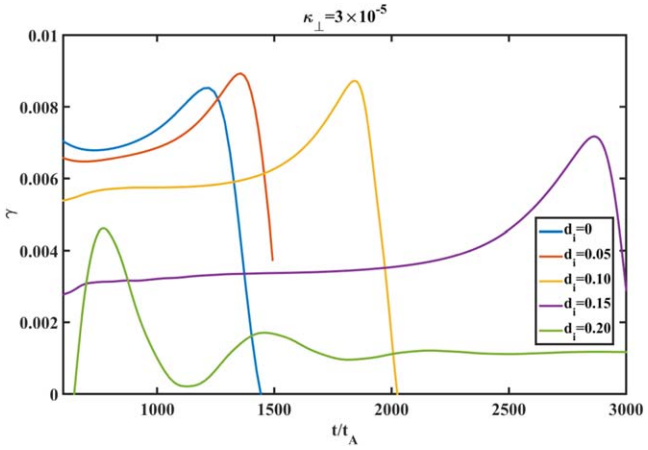

Figure 14. The evolutions of the growth rates with $\kappa_\perp = 3 \times 10^{-5}$ and different d_i. For the cases with $d_i < 0.05$, the maximum nonlinear growth rate slightly increases with increasing d_i. After that, the maximum nonlinear growth strongly decreases with increasing d_i.

influence on the maximum growth rate and the critical value of d_i, which both decrease with increasing $\kappa_\perp$.

4. Summary

The influence of the Hall effect on the nonlinear evolution of the $m/n = 1/1$ resistive-kink mode is investigated. It is found that the Hall effect can lead to the explosive growth of the resistive-kink mode at the nonlinear stage, which is consistent with earlier theoretical predictions [16]. The explosive nonlinear growth mainly results from the structural transition of the current sheet. In the framework of resistive-MHD, the current sheet remains in a Y-type geometry in the entire simulation period. However, the current sheet turns into X-type at the nonlinear stage from Y-type at the linear stage in the Hall-MHD simulation, resulting in the significant acceleration of the reconnection process. The nonlinear explosive growth of the $m/n = 1/1$ resistive-kink mode can be the right candidate to explain the fast pressure crash observed in large tokamaks [8, 9].

It should be noted that the maximum nonlinear growth rate does not always increase with increasing ion inertial length (d_i). There exists a critical value. If d_i is smaller than the critical value, the maximum growth rate increases with increasing d_i; if d_i exceeds the critical value, the maximum growth rate decreases with increasing d_i. It results from the competition between the acceleration of magnetic reconnection due to the decoupling motions of ions and electrons and the suppression by the electron diamagnetic rotation in the Hall MHD. The critical value of d_i decreases with increasing the thermal conductivity $\kappa_\perp$. For $\kappa_\perp = 3 \times 10^{-6}$, the critical value of the ion inertial length is $d_i = 0.12$. It also should be noted that the maximum growth rate also strongly depends on the perpendicular thermal conductivity.

Acknowledgments

This work is supported by the National Natural Science Foundation of China under Grant No. 11775188 and 11835010, the Special Project on High-performance Computing under the National Key R&D Program of China No. 2016YFB0200603, Fundamental Research Fund for Chinese Central Universities.

ORCID iDs

W Zhang https://orcid.org/0000-0001-5859-6298
Z W Ma https://orcid.org/0000-0001-6199-9389
H W Zhang https://orcid.org/0000-0003-1342-5756

References

[1] Von Goeler S, Stodiek W and Sauthoff N 1974 Studies of internal disruptions and $m = 1$ Oscillations in tokamak discharges with soft—x-ray tecniques *Phys. Rev. Lett.* **33** 1201–3
[2] McGuire K and Robinson D C 1979 Sawtooth oscillations in a small tokamak *Nucl. Fusion* **19** 505
[3] Dubois M A, Pecquet A L and Reverdin C 1983 Internal disruptions in the TFR tokamak: a phenomenological analysis *Nucl. Fusion* **23** 147
[4] Igochine V *et al* 2014 Conversion of the dominantly ideal perturbations into a tearing mode after a sawtooth crash *Phys. Plasmas* **21** 110702
[5] Buttery R J, Hender T C, Howell D F, Haye R J L, Sauter O and Testa D 2003 Onset of neoclassical tearing modes on JET *Nucl. Fusion* **43** 69
[6] Chapman I T 2011 Controlling sawtooth oscillations in tokamak plasmas *Plasma Phys. Control. Fusion* **53** 013001
[7] Kadomtsev B 1975 Disruptive instability in tokamaks *Sov. J. Plasma Phys.* **1** 710–5
[8] Edwards A W *et al* 1986 Rapid collapse of a plasma sawtooth oscillation in the JET tokamak *Phys. Rev. Lett.* **57** 210–3

[9] McGuire K *et al* 1990 High-beta operation and magnetohydrodynamic activity on the TFTR tokamak *Phys. Fluids* B **2** 1287–90

[10] Wesson J A 1986 Sawtooth oscillations *Plasma Phys. Control. Fusion* **28** 243

[11] Kolesnichenko Y I, Yakovenko Y V, Anderson D, Lisak M and Wising F 1992 Sawtooth oscillations with the central safety factor, q_0, below unity *Phys. Rev. Lett.* **68** 3881–4

[12] Chapman I T, Scannell R, Cooper W A, Graves J P, Hastie R J, Naylor G and Zocco A 2010 Magnetic reconnection triggering magnetohydrodynamic instabilities during a sawtooth crash in a tokamak plasma *Phys. Rev. Lett.* **105** 255002

[13] Lichtenberg A J, Itoh K, Itoh S I and Fukuyama A 1992 The role of stochasticity in sawtooth oscillations *Nucl. Fusion* **32** 495

[14] Porcelli F, Boucher D and Rosenbluth M N 1996 Model for the sawtooth period and amplitude *Plasma Phys. Control. Fusion* **38** 2163

[15] Aydemir A Y 1992 Nonlinear studies of $m = 1$ modes in high-temperature plasmas *Phys. Fluids* B **4** 3469–72

[16] Wang X and Bhattacharjee A 1993 Nonlinear dynamics of the $m = 1$ instability and fast sawtooth collapse in high-temperature plasmas *Phys. Rev. Lett.* **70** 1627–30

[17] Günter S, Yu Q, Lackner K, Bhattacharjee A and Huang Y M 2015 Fast sawtooth reconnection at realistic Lundquist numbers *Plasma Phys. Control. Fusion* **57** 014017

[18] Breslau J A, Jardin S C and Park W 2007 Three-dimensional modeling of the sawtooth instability in a small tokamak *Phys. Plasmas* **14** 056105

[19] Beidler M T and Cassak P A 2011 Model for incomplete reconnection in sawtooth crashes *Phys. Rev. Lett.* **107** 255002

[20] Beidler M T, Cassak P A, Jardin S C and Ferraro N M 2017 Local properties of magnetic reconnection in nonlinear resistive- and extended-magnetohydrodynamic toroidal simulations of the sawtooth crash *Plasma Phys. Control. Fusion* **59** 025007

[21] Halpern F D, Leblond D, Lütjens H and Luciani J F 2010 Oscillation regimes of the internal kink mode in tokamak plasmas *Plasma Phys. Control. Fusion* **53** 015011

[22] Halpern F D, Lütjens H and Luciani J-F 2011 Diamagnetic thresholds for sawtooth cycling in tokamak plasmas *Phys. Plasmas* **18** 102501

[23] Fischer R, Bock A, Burckhart A, Ford O P, Giannone L, Igochine V, Weiland M and Willensdorfer M 2019 Sawtooth induced q-profile evolution at ASDEX Upgrade *Nucl. Fusion* **59** 056010

[24] Krebs I, Jardin S C, Günter S, Lackner K, Hoelzl M, Strumberger E and Ferraro N 2017 Magnetic flux pumping in 3D nonlinear magnetohydrodynamic simulations *Phys. Plasmas* **24** 102511

[25] Mironov M I, Zaitsev F S, Gorelenkov N N, Afanasyev V I, Chernyshev F V, Nesenevich V G and Petrov M P 2018 Sawtooth mixing of alphas, knock-on D, and T ions, and its influence on NPA spectra in ITAB *Nucl. Fusion* **58** 082030

[26] Guo W, Wang J, Liu D and Wang X 2016 A resistive magnetodynamics analysis of sawtooth driven tearing modes in tokamak plasmas *Phys. Plasmas* **23** 062117

[27] Jardin S C, Ferraro N and Krebs I 2015 Self-organized stationary states of tokamaks *Phys. Rev. Lett.* **115** 215001

[28] Nam Y B, Ko J S, Choe G H, Bae Y, Choi M J, Lee W, Yun G S, Jardin S and Park H K 2018 Validation of the 'full reconnection model' of the sawtooth instability in KSTAR *Nucl. Fusion* **58** 066009

[29] Kim G, Yun G S and Woo M 2019 Mitigation of sawtooth crash as a manifestation of MHD mode coupling prior to disruption of KSTAR plasma *Plasma Phys. Control. Fusion* **61** 055001

[30] Li E, Igochine V, Dumbrajs O, Xu L, Chen K, Shi T and Hu L 2014 The non-resonant kink modes triggering strong sawtooth-like crashes in the EAST tokamak *Plasma Phys. Control. Fusion* **56** 125016

[31] Li G S *et al* 2019 Destabilization of field-line localized density fluctuation with a $1/1$ internal kink mode in the EAST tokamak *Nucl. Fusion* **59** 096032

[32] Aydemir A Y, Kim J Y, Park B H and Seol J 2015 On resistive magnetohydrodynamic studies of sawtooth oscillations in tokamaks *Phys. Plasmas* **22** 032304

[33] Jiang M *et al* 2019 Localized modulation of turbulence by $m/n = 1/1$ magnetic islands in the HL-2A tokamak *Nucl. Fusion* **59** 066019

[34] Ali A and Zhu P 2019 Effects of plasmoid formation on sawtooth process in a tokamak *Phys. Plasmas* **26** 052518

[35] Liu D, Heidbrink W W, Podestà M, Hao G Z, Darrow D S, Fredrickson E D and Kim D 2018 Effect of sawtooth crashes on fast ion distribution in NSTX-U *Nucl. Fusion* **58** 082028

[36] Choe G H, Yun G S, Park H K and Jeong J H 2018 Slow crash in modified sawtooth patterns driven by localized electron cyclotron heating and current drive in KSTAR *Nucl. Fusion* **58** 106038

[37] Ahn J-H, Garbet X, Lütjens H, Marx A, Nicolas T, Sabot R, Luciani J-F, Guirlet R, Février O and Maget P 2016 Non-linear dynamics of compound sawteeth in tokamaks *Phys. Plasmas* **23** 052509

[38] Yu Q, Günter S and Lackner K 2015 Numerical modelling of sawtooth crash using two-fluid equations *Nucl. Fusion* **55** 113008

[39] Brunetti D, Graves J P, Halpern F D, Luciani J F, Lütjens H and Cooper W A 2015 Extended MHD simulations of infernal mode dynamics and coupling to tearing modes *Plasma Phys. Control. Fusion* **57** 054002

[40] Kleiner A, Graves J P, Brunetti D, Cooper W A, Halpern F D, Luciani J F and Lütjens H 2016 Neoclassical tearing mode seeding by coupling with infernal modes in low-shear tokamaks *Nucl. Fusion* **56** 092007

[41] Hazeltine R D, Hsu C T and Morrison P J 1987 Hamiltonian four-field model for nonlinear tokamak dynamics *Phys. Fluids* **30** 3204–11

[42] Parker E N 1957 Sweet's mechanism for merging magnetic fields in conducting fluids *J. Geophys. Res.* **62** 509–20

[43] Ma Z W and Bhattacharjee A 1996 Fast impulsive reconnection and current sheet intensification due to electron pressure gradients in semi-collisional plasmas *Geophys. Res. Lett.* **23** 1673–6

[44] Ma Z W and Bhattacharjee A 1998 Sudden enhancement and partial disruption of thin current sheets in the magnetotail due to Hall MHD effects *Geophys. Res. Lett.* **25** 3277–80

[45] Ma Z and Bhattacharjee A 2001 Hall magnetohydrodynamic reconnection: the geospace environment modeling challenge *J. Geophys. Res.: Space Phys.* **106** 3773–82

[46] Wang X G, Bhattacharjee A and Ma Z W 2000 Collisionless reconnection: effects of Hall current and electron pressure gradient *J. Geophys. Res.: Space Phys.* **105** 27633–48

[47] Jardin S C 2012 Review of implicit methods for the magnetohydrodynamic description of magnetically confined plasmas *J. Comput. Phys.* **231** 822–38

[48] Park W, Belova E V, Fu G Y, Tang X Z, Strauss H R and Sugiyama L E 1999 Plasma simulation studies using multilevel physics models *Phys. Plasmas* **6** 1796–803

[49] Zhang H, Zhu J, Ma Z, Kan G, Wang X and Zhang W 2019 Acceleration of three-dimensional Tokamak magnetohydrodynamical code with graphics processing unit and OpenACC heterogeneous parallel programming *Int. J. Comput. Fluid Dyn.* 1–14

[50] Duan L, Wang X and Zhong X 2010 A high-order cut-cell method for numerical simulation of hypersonic boundary-layer instability with surface roughness *J. Comput. Phys.* **229** 7207–37

[51] Cheng C and Chance M 1987 NOVA: a nonvariational code for solving the MHD stability of axisymmetric toroidal plasmas *J. Comput. Phys.* **71** 124–46

[52] Wang S and Ma Z 2015 Influence of toroidal rotation on resistive tearing modes in tokamaks *Phys. Plasmas* **22** 122504

[53] Wang X G, Bhattacharjee A and Ma Z W 2001 Scaling of collisionless forced reconnection *Phys. Rev. Lett.* **87** 265003

[54] Ara G, Basu B, Coppi B, Laval G, Rosenbluth M and Waddell B 1978 Magnetic reconnection and $m = 1$ oscillations in current carrying plasmas *Ann. Phys.* **112** 443–76

[55] Zhang W, Ma Z W, Zhang H W and Zhu J 2019 Dynamic evolution of resistive kink mode with electron diamagnetic drift in tokamaks *Phys. Plasmas* **26** 042514